Volume 16, Number 2, 2023. pp. 229-237

Jordan Journal of Physics

ARTICLE

Investigation of the Effects of Yb and Nd Doping and Operating Temperature on CeO_2 Photocatalyst Properties

Handan Ö. TORUN[a] and **Rabia KIRKGEÇİT**[b]

[a] *Department of Energy Systems Engineering, Kahramanmaras Istiklal University, Kahramanmaraş, Turkey.*
[b] *Material Science and Engineering, Institute of Science, Kahramanmaraş Sütçü İmam University, Kahramanmaraş, 46050, Turkey.*

Doi: **https://doi.org/10.47011/16.2.10**
Received on: 25/04/2022; *Accepted on: 11/09/2022*

Abstract: This study investigated the effects of the co-doping of Yb and Nd elements and the operating temperature on photocatalytic degradation. Composites of $Ce_{0.96}Nd_{0.04}O_2$ (CN), $Ce_{0.96}Yb_{0.04}O_2$ (CY), and $Ce_{0.92}Nd_{0.04}Yb_{0.04}O_2$ (CNY) were obtained by self-propagating room temperature reaction method, involving several sequential steps. The composites were sintered at 500 and 600 °C. The structural and morphological properties of the compounds were examined via X-ray powder diffractometry (XRD), scanning electron microscopy (SEM), Raman spectroscopy, and UV-vis spectroscopy. In the degradation study, methylene blue was chosen as the dyestuff. Although the operating temperature affected the degradation negatively, co-doping had a positive effect. The lowest bandgap (2.70 eV) was found for the CNY compound and the CNY without applied operating temperature had the highest percentage of degradation (80.76%).

Keywords: CeO_2, Self-propagating reaction, Co-doping, Photocatalytic, Rare earth element.

1. Introduction

Without proper disposal of dyestuffs by the textile industry, their release causes serious environmental pollution. Photocatalytic methods are frequently used for dyestuff removal. For this purpose, metal oxide compounds are used as photocatalysts. To date, those that have been highly studied include ZnO, TiO_2, and Fe_2O_3 [1-5]. Recently, the photocatalytic properties of CeO_2 have begun to draw attention because CeO_2 is a non-toxic rare earth metal oxide compound having a wide bandgap. In the crystal lattice, oxygen is four-coordinated and cerium is eight-coordinated and it has an empty 4f orbital. In addition, the oxygen vacancies formed in the structure as a result of the redox reaction between $Ce^{4+/}Ce^{3+}$ along with absorption in the visible region make it a good photocatalyst candidate [6, 7].

Different elements are doped into the CeO_2 crystal structure in order to reduce the bandgap and increase the photocatalyst efficiency. Miao et al. studied F-doped CeO_2 and found that F increased pure CeO_2 degradation 5.5-fold [8]. Liyanage et al. investigated the catalysis and degradation of two different dyestuffs by doping CeO_2 with Y at different mole ratios. They found that as the contribution rate increased, the percentage of degradation decreased [9]. Xu et al. investigated Y, Nd, La, and Sm-doped CeO_2 in bisphenol A (BPA) degradation and acetaldehyde degradation efficiency. They found Sm-doped CeO_2 to be three and five times more effective compared to the others and pure CeO_2 [10].

Corresponding Author: Handan ÖZLÜ TORUN **Email**: handanozlu@gmail.com

Until now, numerous CeO_2 photocatalyst degradation studies have been carried out on pH, dyestuff concentration, and concentration variation. However, studies in the literature on operating temperature are limited. In this study, the effect of operating temperature was investigated by using CeO_2 compounds and methylene blue (MB) dyestuff. Because the compounding of the selected Yb and Nd ions has been little studied, the compounds were synthesized by the self-propagating room temperature synthesis method. The effects of both co-doping and operating temperature on the photocatalysis results were compared and discussed.

2. Material and Methods

2.1. Material

The compounds $Ce_{0.96}Nd_{0.04}O_2$ (CN), $Ce_{0.96}Yb_{0.04}O_2$ (CY), and $Ce_{0.92}$ $Nd_{0.04}$ $Yb_{0.04}O_2$ (CNY) were synthesized by self-propagating room temperature synthesis (SPRT). According to the information we have obtained from the literature, this method is effective in terms of cost and time [11-13]. It is a reaction between metal nitrates and sodium hydroxide in the SPRT method. It does not require any additional temperature treatments of the chelator as in the sol-gel method. The starting reactants used were $Ce(NO_3)3{\cdot}6H_2O$ (Aldrich, 99.999%), $Nd(NO_3)3{\cdot}5H_2O$ (Aldrich, 99.999%), $Yb(NO_3)3{\cdot}5H_2O$ (Aldrich, 99.999%), and NaOH. The starting compounds weighed in calculated amounts and were dissolved in distilled water according to the experimental flow chart given in Fig. 1. Afterward, 3 mL of 6M NaOH was added dropwise and left to complete the reaction. The heterogeneous mixture of shampoo consistency was centrifuged, and the remainder was filtered, washed several times in distilled water and alcohol, and dried at room temperature. The resulting powders were sintered at 500 °C for 6 h and at 600 °C for 3 h.

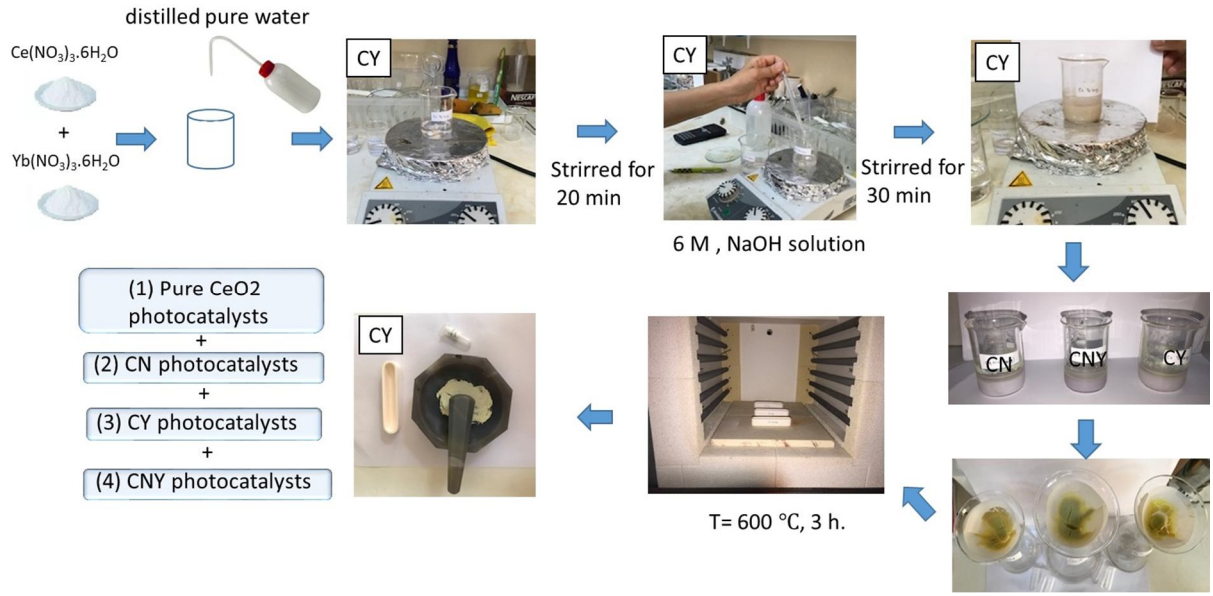

FIG. 1. Process steps of self-propagating room temperature synthesis.

2.2. Method

The X-ray diffraction (XRD) technique was used to examine the crystal structure and phase purity. The calcined powders were examined via XRD (Philips X 'Pert Pro, $\lambda = 0.154056$ nm, Cu-Kα radiation). The μ-Raman spectroscopy analysis was performed for 2 s at room temperature using a portable Raman spectrometer (BWS465 B.W. Tech. Inc.) with a 1300-100 cm^{-1} 785 nm He-Ne laser. The Zeiss EVO 10 LS scanning electron microscope (SEM) was used to define the morphology and microstructure of the samples, and energy dispersive X-ray (EDX) analysis was performed to evaluate the elemental surface. Photocatalytic behavior was investigated via UV spectroscopy (UV-1800 Shijadzu UV spectrophotometer).

For photocatalytic properties, methylene blue (MB) was used as a degrading dye, and the effect of the operating temperature of undoped and doped CeO_2 compounds was investigated. A 300-watt xenon lamp was used as the light

source. The distance between the sample and the light source is about 10 cm. Photocatalytic degradation measurements were made in the range of 350-800 nm in UV-Vis spectroscopy. Dyestuff solution (MB) 50 mL, 5 ppm (mgL^{-1}) aqueous solution was prepared for degradation measurement. 30 mg of catalyst was used for each run. In determining the effect of operating temperature, samples containing dyestuff and catalyst were heat treated at 60 °C for 1 hour. Immediately after the application, it was kept in the dark for approximately 30 minutes for the adsorption-desorption equilibrium. Then, 2 ml samples were taken every 10 minutes from 0 to 90, and their measurements were taken by scanning in UV-Vis spectroscopy. Calculations were made using methylene blue dye's maximum absorbance at 664 nm. The degradation efficiency was calculated using Eq. (1).

$$.\%\ DE = C_o\text{-}C/C_o \times 100 \quad (1)$$

where C_o is the initial concentration and C is the concentration obtained at 90 min.

3. Results and Discussion

3.1. XRD

The XRD pattern of the compounds obtained is shown in Fig. 2. The samples were examined via XRD and the data of the samples after drying at room temperature showed that the CeO_2 peaks were weak due to impurities. The desired cubic crystal structure had not been formed. The weak form of the crystal can be due to the reaction products given in Eq. (1). According to the thermal analysis results, Boskovic et al. reported that the impurities were completely removed after 300°C [11]. These undesirable impurities were removed by washing and temperature treatments. Although CeO_2 peaks were observed at 500 °C, better crystal structure formation results were obtained at 600 °C. It can be seen that the XRD patterns obtained at this temperature are quite similar to the cubic structure encountered in the literature [14-16].

$$2[(1-x)Ce(NO_3)_3\cdot 6H_2O + xM(NO_3)_3\cdot 6H_2O] + 6NaOH + (1/2-\delta)O_2 \rightarrow 2Ce_{1-x}M_xO_{2-\delta} + 6NaNO_3 + 15H_2O \quad (2)$$

Figure 3 shows that the cubic crystal lattice of the pure CeO_2 was not disturbed by doping. The temperature increase was effective in the formation of the cubic structure.

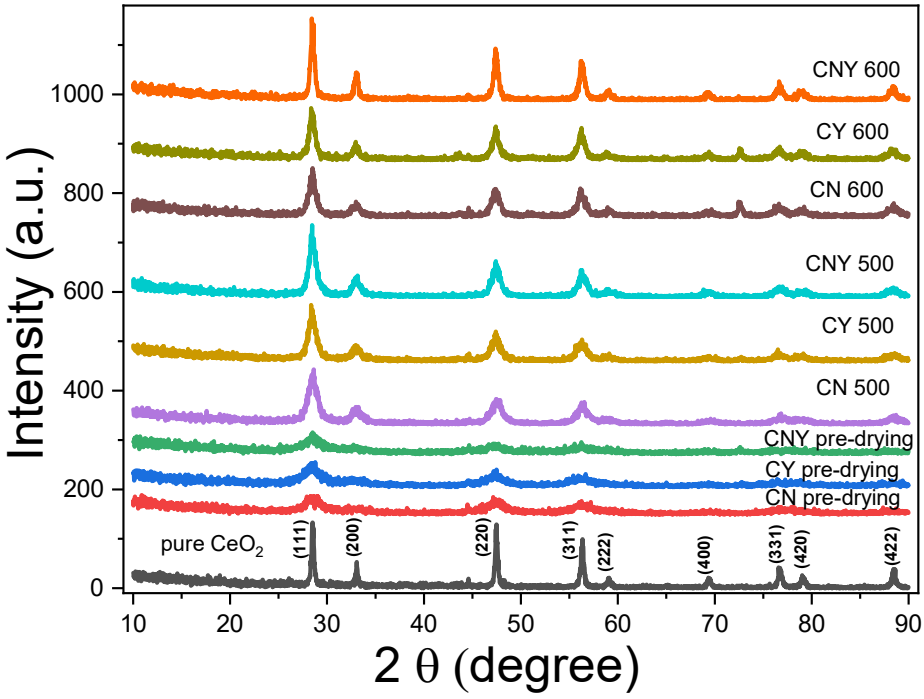

FIG. 2. XRD pattern of all composites.

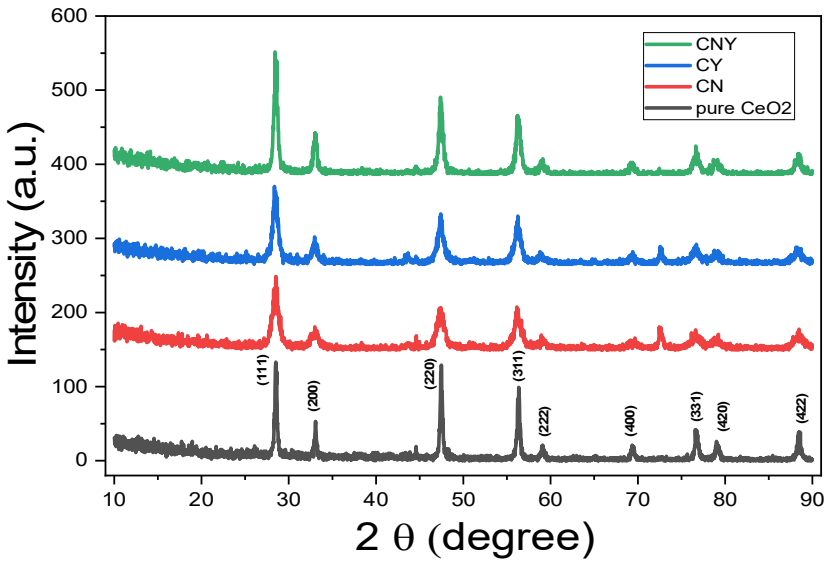

FIG. 3. XRD pattern at 600 °C.

X-ray diffraction line broadening is known to be affected by crystallite size and internal stresses. Therefore, to evaluate parameters, the crystal size was calculated using the following Debye Scherrer methods [Eqs. (3) and (4)], taking the peaks with the highest relative intensity as a reference:

$$D = k \cdot \lambda / \beta \cdot \cos \theta \quad (3)$$

$$\beta = \beta_{obs} - \beta_{std} \quad (4)$$

D is the consistent scattering length (crystal size); k is the Debye Scherrer constant (0.89); λ is the wavelength of the energy; β' is the FWHM value and θ' is the Bragg angle. The crystal sizes of the compounds after sintering at 600 °C were calculated by the Debye Scherrer equation using X'Pert HighScore Plus software. The physical properties of the samples are summarized in Table 1.

TABLE 1. Properties of composites at 600 °C.

Sample	Ref. Code	Crystallite Size (nm)	MicroStrain (%)	Crystal System	Space Group	Particle Size (µm)
pure CeO_2	98005434 2	33.3	0.430	Cubic	Fm-3m	0.14
CN		12.73	1.226	Cubic	Fm-3m	0.16
CY		19.00	1.201	Cubic	Fm-3m	0.34
CNY		24.60	0.575	Cubic	Fm-3m	0.35

3.2. SEM

Morphological results of the composites obtained as a result of 600 °C heat treatment are given in Fig. 4. The particles were found to be clustered and spherical. In addition, the particle size calculated using the ImageJ program varied in the range of 140-350 nm. Particle sizes are among the prominent parameters in degradation studies.

3.3. Raman Analysis

Raman spectroscopy is one of the methods that gives information about crystal structure and defect formation. Raman results for the samples synthesized at 600 °C are given in Fig. 5. The peak at 460 cm^{-1} is characteristic of the CeO_2 cubic lattice [17]. With doping, the new shifts with very low intensity at approximately 425 cm^{-1} and 550 cm^{-1} indicate the formation of oxygen voids in the structure [18]. The very low intensity was attributed to the low mole values of the additive types.

Oxygen vacancy formation can be explained by the following mechanism [19].

$$M_2O_3 + CeO_2 \longrightarrow 2M_{ce2} + VO\bullet\bullet + 3O^O$$

According to the mechanism, the additive type settles in the Ce^{4+} position and an oxygen vacancy is formed in the crystal structure.

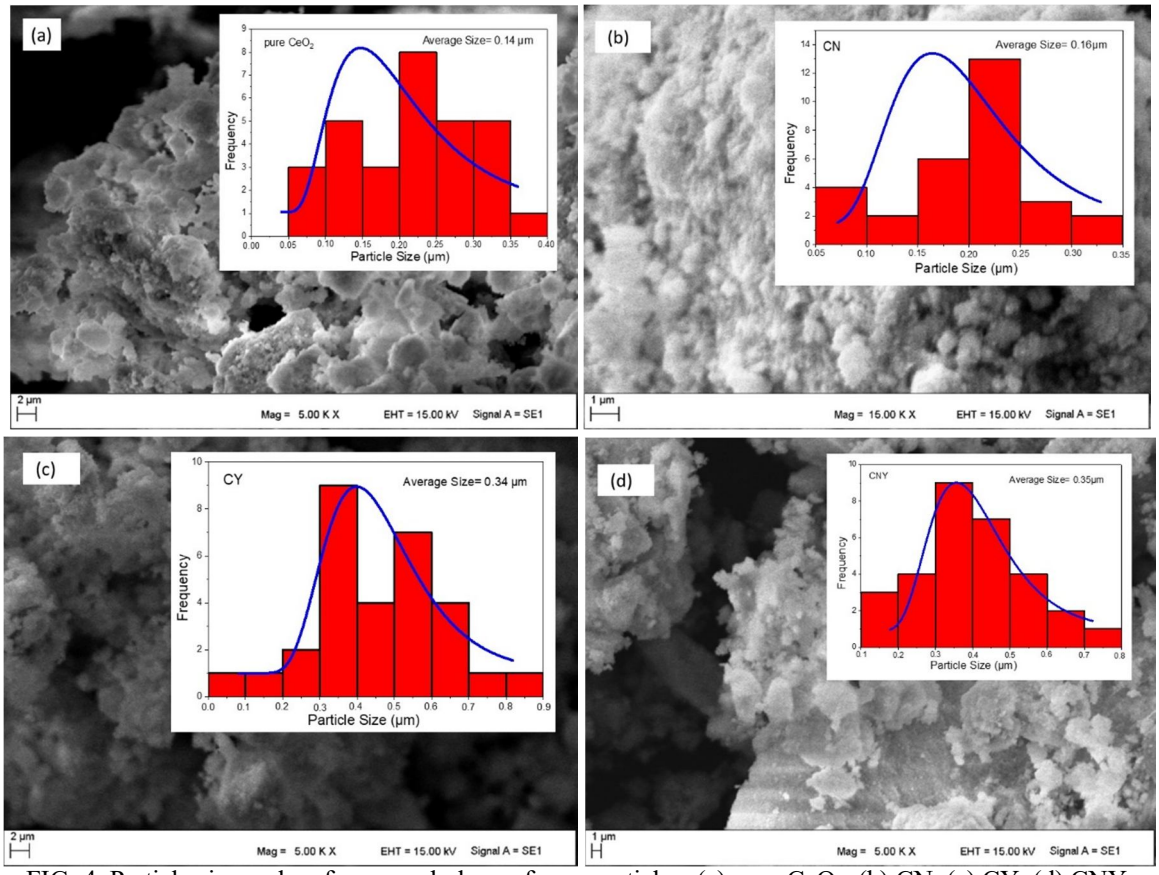

FIG. 4. Particle size and surface morphology of nanoparticles: (a) pure CeO_2, (b) CN, (c) CY, (d) CNY.

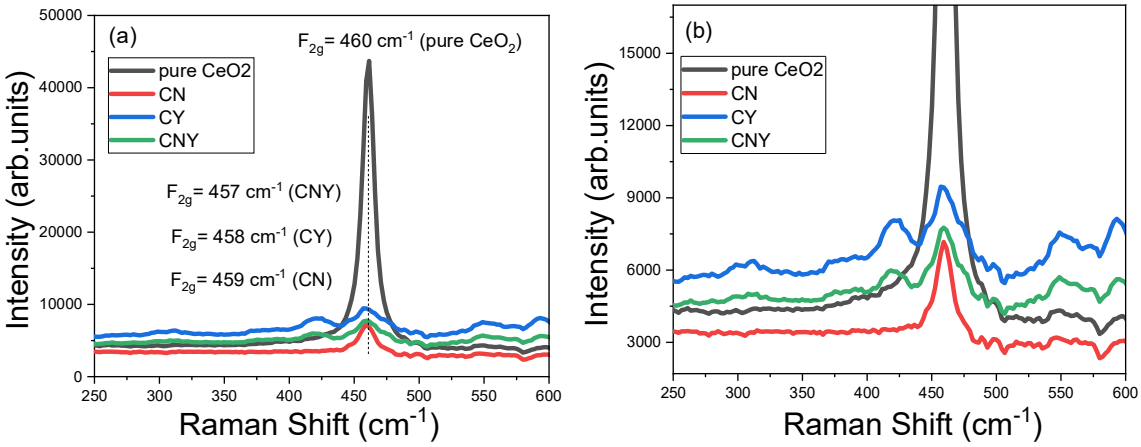

FIG. 5. Raman spectra of pure CeO_2, CN, CY, and CNY.

3.4. UV-Vis Analysis

Many degradation studies have examined the amount of catalysis, the type of catalysis, and the operating conditions, as detailed in the Introduction section. In this study, the effect of the catalysis type and operating conditions on dye degradation was addressed. Accordingly, methylene blue (MB), a cationic dye, was used in the UV-vis study. Pure CeO_2, CN, CY, and CNY compounds were established as photocatalysts. In determining the effect of the operating temperature, samples containing dyestuff and catalyst were heat-treated at 60 °C for 1 h. Mixtures with/without 5 ppm MB and 30 mg catalyst were kept in the dark for 30 min. The measurement intervals were determined as 10 min and the total time as 90 min. The absorbance curves of the samples kept at room temperature and subjected to heat treatment are given in Fig. 6.

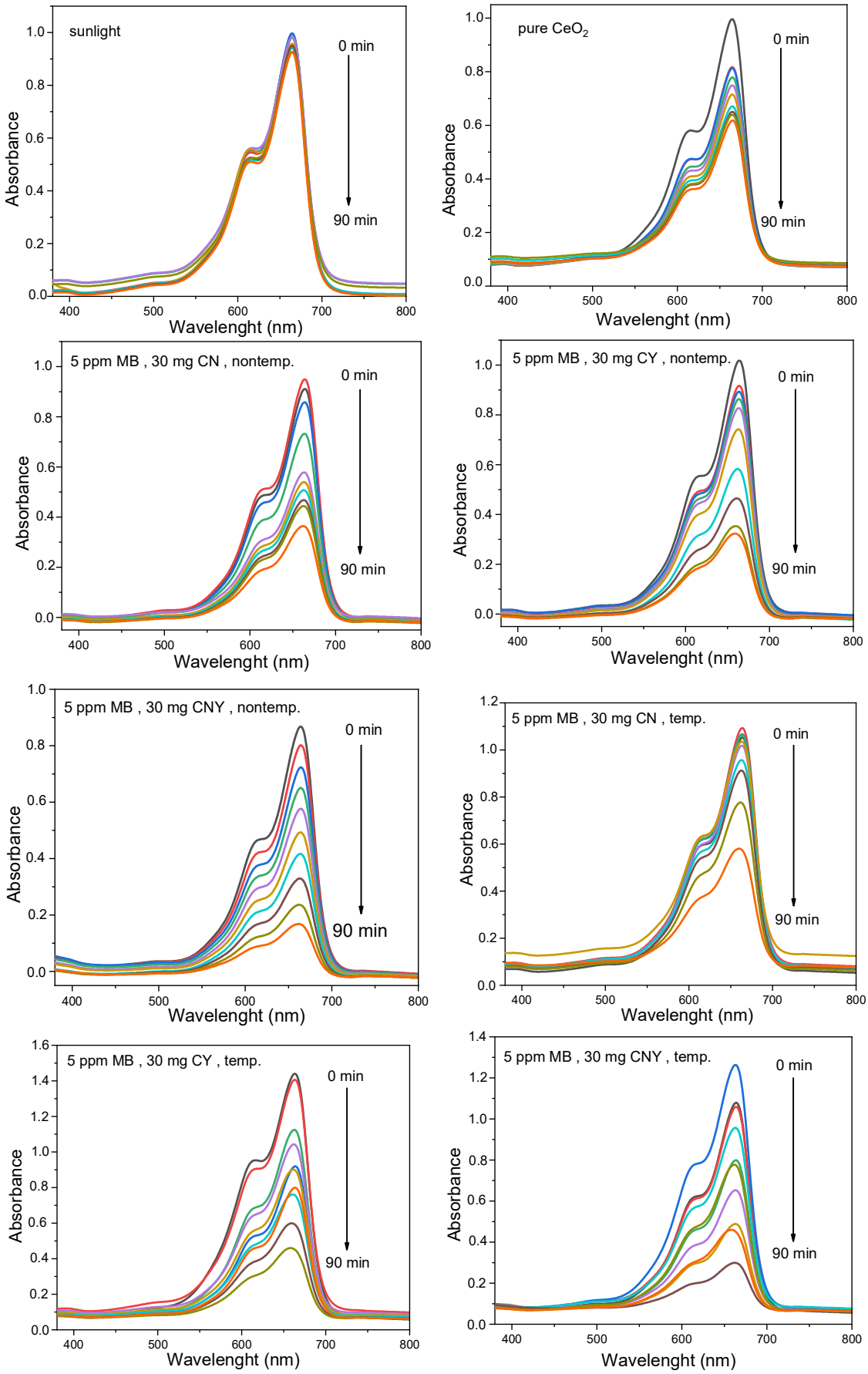

FIG. 6. Degradation activity of 30-mg CN, CY, CNY photocatalysts: Samples at room temperature (nontemp) and heated to 60 °C (temp).

The graphics given in Fig. 6 demonstrate the dyestuff decomposition over time. The decrease in the degradation curves of the dye samples without a photocatalyst was minimal. This illustrates that the synthesized compounds had an effect on degradation. Decomposition in samples containing a catalyst can be explained in terms of the reaction mechanism. In this mechanism, the dyestuff is adsorbed in the photocatalyst candidate compound. The effect of light then forms electrons and holes. As the reaction continues, free OH and oxygen radicals are formed. These radicals are adsorbed over the dyestuff. Oxygen vacancies created in the CeO_2 crystal structure are important for the formation of the mechanism [20-22].

CeO_2-dye + hV (energy) $\longrightarrow$ CeO_2(e-,h+)-dye

$H_2O + h^+ \longrightarrow OH^-$ (radical) + H^+

$O_2 + e^- \longrightarrow O_2^-$ (superoxide radical)

$O_2^- + H^+ \longrightarrow H_2O$

The results obtained in MB degradation studies are summarized in Table 2.

TABLE 2. Photocatalysis results of CN, CY, and CNY samples.

Particle	Apparent rate constant 'k' (min^{-1})	Bandgap (eV)	Band Edge (nm)	Efficiency 'η' (%)
Simulated light MB (particle-free)	0.00092	-	-	7.12
Pure CeO_2	0.00463	3.00	304	38.05
CN non-temp	0.01175	2.93	310	61.74
CY non-temp	0.01331	2.79	316	69.05
CNY non-temp	0.01749	2.70	322	80.76
CN temp	0.01005	-	-	47.57
CY temp	0.00554	-	-	44.47
CNY temp	0.01086	-	-	58.48

According to Table 2, an increase in the percentage of dye degradation removal was observed when only Yb and only Nd were added to the CeO2 crystal lattice. However, the highest efficiency was obtained with the co-doping of Yb and Nd. The degradation rate was 38% for pure CeO_2, whereas it increased to 80.76% for the Yb and Nd-doped compounds. Thus, the co-doping method in the study had a positive effect on the degradation. This is called the synergistic effect [20]. As a result of the synergistic effect, it is seen that the compound formed when Yb and Nd are doped together with equal mole ratios to pure CeO_2 has an optical band gap of 2.70 eV. It has been the focus of many current studies. In the synergistic effect, ternary structures formed with different elements have begun to attract attention, with Ag and Ag compounds and Bi_2O_3 and $BiVO_4$ compounds standing out [23]. For example, in the previous study conducted by our study group, Dy and La were used together, and the degradation was found to be 60% [24].

Again, when the data in Fig. 7 and Table 2 are compared, degradation was reduced in the samples that were kept at 60 °C before UV measurements compared to those that were not subjected to heat treatment. Although studies in the literature on operating temperature are limited, the results are varied. In the photocatalysis study of the MoO_3 compound by Chithambarara et al., operating temperatures of 45 and 65 °C were chosen, and the degradation efficiency was improved by 8% [25]. On the other hand, Chen investigated the azo dyestuff degradation of TiO_2 in the 15-40 °C range and observed that the degradation increased with the increase in temperature [26]. Studies have reported that the dye degradation efficiency does not change when the temperature of the dye solution changes [27]. However, in this study with CeO_2, the temperature was observed to have a negative effect. As the operating temperature approaches the boiling point of water, desorption tends to inhibit the reaction. Therefore, it also negatively affects the adsorption of the final reaction product. The efficiency of the photocatalyst is reduced [28.].

Regarding the relationship between particle size and degradation, the degradation of the CNY compound, which had the largest particle size, was found to be high because a larger surface area increases adsorption.

With doping, a decrease in the optical (Tauc) bandgap of pure CeO_2 was observed (Fig. 8).

The Nd-Yb ions had the lowest bandgap when doped together. The low optical bandgap in the heat-treated samples resulted in the highest degradation. The reduction of the optical bandgap facilitated the e-transition between the conduction band and the valence band [23].

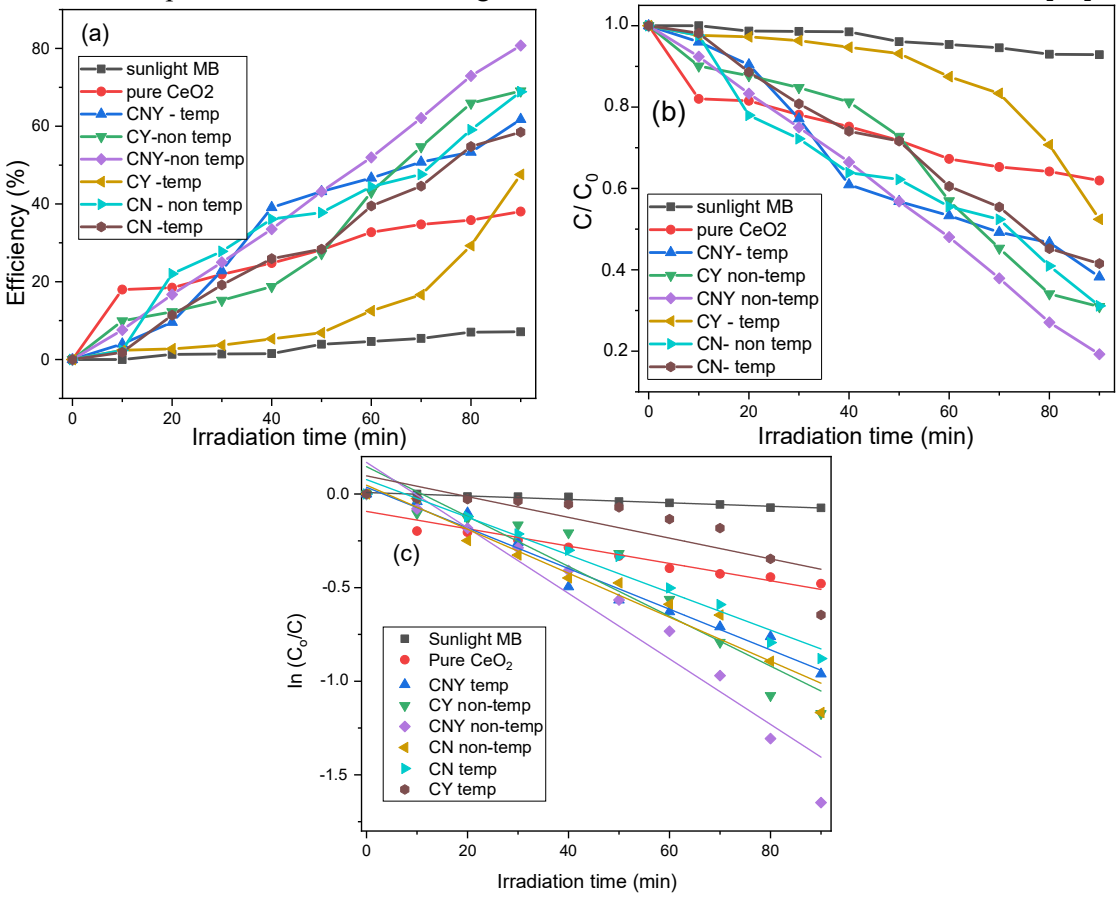

FIG. 7. Pure CeO_2, CN, CY, and CNY nanoparticles: (a-b) photodegradation efficiency, (c) kinetics.

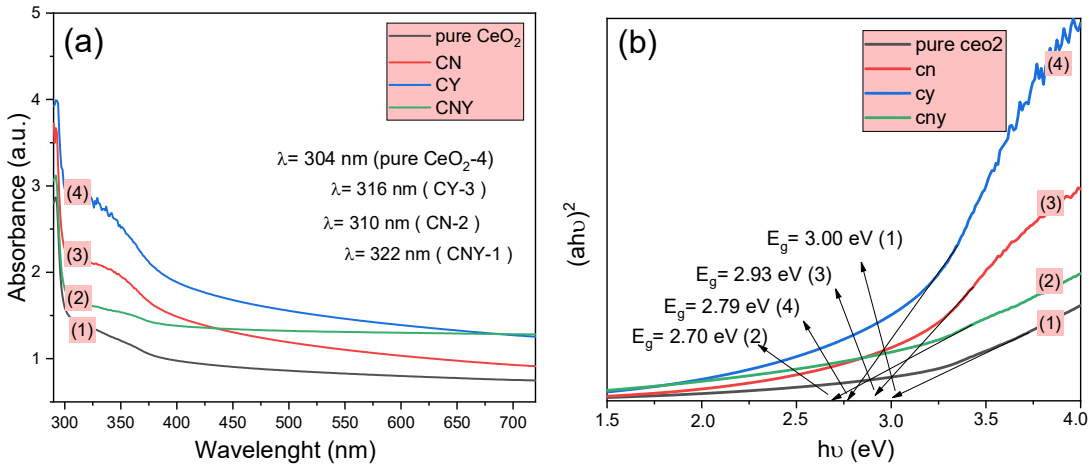

FIG. 8. (a) Absorbance and (b) Tauc plot bandgap of CN, CY, and CNY samples.

4. Conclusions

This study has reported the effects of the type of additive and the doping method on photocatalytic efficiency. According to XRD results, all compounds prepared by the self-propagating room temperature synthesis method were found to have the face-centered cubic (FCC) structure. Nanocrystalline-sized compounds were obtained. It was determined that co-doping created a synergistic effect in the Yb, Nd, and Yb-Nd additives. The selected treatment temperatures and times reduced the degradation efficiency by about one-third. It was concluded that $Ce_{0.92}Nd_{0.04}Yb_{0.04}O_2$ (CNY) has the highest degradation efficiency (80.76%) and the lowest bandgap (2.70).

References

[1] Kerli, S., Soğuksu, A.K. and Kavgacı, M., Reaction Kinetics, Mechanisms and Catalysis, 134 (2021) 539.

[2] Kerli, S. and Soğuksu, A.K., Zeitschrift für Kristallographie-Crystalline Materials, 234 (11-12) (2019) 725.

[3] Dokan, F.K. and Kuru, M., Journal of Materials Science: Materials in Electronics, 32 (1) (2021) 640.

[4] Veziroglu, S., Kuru, M., Ghori, M.Z., Dokan, F.K., Hinz, A.M., Strunskus, T.,... and Aktas, O.C., Materials Letters, 209 (2017) 486.

[5] Chen, X., Wu, Z., Liu, D. and Gao, Z., Nanoscale Research Letters, 12 (1) (2017) 1.

[6] Chinnu, M.K., Anand, K.V., Kumar, R.M., Alagesan, T. and Jayavel, R., Materials Letters, 113 (2013) 170.

[7] Choudhury, B. and Choudhury, A., Materials Chemistry and Physics, 131 (3) (2012) 666.

[8] Miao, H., Huang, G.F., Liu, J.H., Zhou, B.X., Pan, A., Huang, W.Q. and Huang, G.F., Applied Surface Science, 370 (2016) 427.

[9] Liyanage, A.D., Perera, S.D., Tan, K., Chabal, Y. and Balkus Jr, K.J., Acs Catalysis, 4 (2) (2014) 577.

[10] Xu, B., Yang, H., Zhang, Q., Yuan, S., Xie, A., Zhang, M. and Ohno, T., Chem. Cat. Chem., 12 (9) (2020) 2638.

[11] Boskovic, S., Djurovic, D., Dohcevic-Mitrovic, Z., Popovic, Z., Zinkevich, M. and Aldinger, F., Journal of Power Sources, 145 (2) (2005) 237.

[12] Matović, B., Stojmenović, M., Pantić, J., Varela, A., Žunić, M., Jiraborvornpongsa, N. and Yano, T., Journal of Asian Ceramic Societies, 2 (2) (2014) 117.

[13] Stojmenović, M., Bošković, S., Zec, S., Babić, B., Matović, B., Bučevac, D., and Aldinger, F., Journal of Alloys and Compounds, 507 (1) (2010) 279.

[14] Malleshappa, J., Nagabhushana, H., Sharma, S.C., Sunitha, D.V., Dhananjaya, N., Shivakumara, C. and Nagabhushana, B.M., Journal of alloys and compounds, 590 (2014) 131.

[15] Bakir, A.H. and TORUN, H.Ö., Journal of the Chemical Society of Pakistan, 43 (6) (2021) 314.

[16] Matović, B., Dukić, J., Babić, B., Bučevac, D., Dohčević-Mitrović, Z., Radović, M. and Bošković, S., Ceramics International, 39 (5) (2013) 5007.

[17] Kim, N.W., Lee, D.K. and Yu, H., RSC Advances, 9 (24) (2019) 13829.

[18] Taniguchi, T., Watanabe, T., Sugiyama, N., Subramani, A.K., Wagata, H., Matsushita, N. and Yoshimura, M., The Journal of Physical Chemistry C, 113 (46) (2009) 19789.

[19] Torun, H.O. and Çakar, S., Journal of Thermal Analysis and Calorimetry, 133 (3) (2018) 1233.

[20] Fauzi, A.A., Jalil, A.A., Hassan, N.S., Aziz, F.F.A., Azami, M.S., Hussain, I.,... and Vo, D.V., Chemosphere, 286 (1) (2022) 131651.

[21] Kirkgeçit, R., Torun, H.Ö., Dokan, F.K. and Öztürk, E., Journal of Photochemistry and Photobiology A: Chemistry, 423 (2021) 113602.

[22] Gao, H., Yang, H., Yang, G. and Wang, S., Materials Technology, 33 (5) (2018) 321.

[23] Ma, R., Zhang, S., Wen, T., Gu, P., Li, L., Zhao, G., … and Wang, X., Catalysis Today, 335 (2019) 20.

[24] Torun, H.Ö., Kırkgeçit, R., Dokan, F.K. and Öztürk, E., Journal of Photochemistry and Photobiology A: Chemistry, 418 (2021) 113338.

[25] Chithambararaj, A., Sanjini, N.S., Velmathi, S. and Bose, A.C., Physical Chemistry Chemical Physics, 15 (35) (2013) 14761.

[26] Chen, C.Y., Water, Air and Soil Pollution, 202 (1) (2009) 335.

[27] Huang, Y., Cui, C., Zhang, D., Li, L. and Pan, D., Chemosphere, 119 (2015) 295.

[28] Elkady, M.F. and Hassan, H.S., Polymers, 13 (13) (2021) 2033.